Published in "American Journal of Physiology: Renal Physiology 294(6): F1373-F1380, 2008" which should be cited to refer to this work.

Mouse model of type II Bartter's syndrome. II. Altered expression of renal sodium- and water-transporting proteins

Carsten A. Wagner,[1]* Dominique Loffing-Cueni,[2,3]* Qingshang Yan,[4] Nicole Schulz,[1] Panagiotis Fakitsas,[1] Monique Carrel,[2,3] Tong Wang,[4] Francois Verrey,[1] John P. Geibel,[4,5] Gerhard Giebisch,[4] Steven C. Hebert,[4] and Johannes Loffing[2,3]

[1]*Institute of Physiology, Center of Integrative Human Physiology, and* [2]*Institute of Anatomy, University of Zurich, Zurich;* [3]*Department of Medicine, Unit of Anatomy, University of Fribourg, Fribourg, Switzerland; and Departments of* [4]*Cellular and Molecular Physiology and* [5]*Surgery, Yale Medical School, New Haven, Connecticut*

Wagner CA, Loffing-Cueni D, Yan Q, Schulz N, Fakitsas P, Carrel M, Wang T, Verrey F, Geibel JP, Giebisch G, Hebert SC, Loffing J. Mouse model of type II Bartter's syndrome. II. Altered expression of renal sodium- and water-transporting proteins. *Am J Physiol Renal Physiol* 294: F1373–F1380, 2008. First published March 5, 2008; doi:10.1152/ajprenal.00613.2007.—Bartter's syndrome represents a group of hereditary salt- and water-losing renal tubulopathies caused by loss-of-function mutations in proteins mediating or regulating salt transport in the thick ascending limb (TAL) of Henle's loop. Mutations in the ROMK channel cause type II antenatal Bartter's syndrome that presents with maternal polyhydramnios and postnatal life-threatening volume depletion. We have developed a colony of *Romk null* mice showing a Bartter-like phenotype and with increased survival to adulthood, suggesting the activation of compensatory mechanisms. To test the hypothesis that upregulation of Na^+-transporting proteins in segments distal to the TAL contributes to compensation, we studied expression of salt-transporting proteins in ROMK-deficient ($Romk^{-/-}$) mice. Plasma aldosterone was 40% higher and urinary PGE_2 excretion was 1.5-fold higher in $Romk^{-/-}$ compared with wild-type littermates. Semiquantitative immunoblotting of kidney homogenates revealed decreased abundances of proximal tubule Na^+/H^+ exchanger (NHE3) and Na^+-P_i cotransporter (NaPi-IIa) and TAL-specific Na^+-K^+-$2Cl^-$-cotransporter (NKCC2/BSC1) in $Romk^{-/-}$ mice, while the distal convoluted tubule (DCT)-specific Na^+-Cl^- cotransporter (NCC/TSC) was markedly increased. The abundance of the α-,β-, and γ-subunits of the epithelial Na^+ channel (ENaC) was slightly increased, although only differences for γ-ENaC reached statistical significance. Morphometry revealed a fourfold increase in the fractional volume of DCT but not of connecting tubule (CNT) and collecting duct (CCD). Consistently, CNT and CD of $Romk^{-/-}$ mice revealed no apparent increase in the luminal abundance of the ENaC compared with those of wild-type mice. These data suggest that the loss of ROMK-dependent Na^+ absorption in the TAL is compensated predominately by upregulation of Na^+ transport in downstream DCT cells. These adaptive changes in $Romk^{-/-}$ mice may help to limit renal Na^+ loss, and thereby, contribute to survival of these mice.

thick ascending limb of Henle's loop; distal convoluted tubule; thiazide-sensitive NaCl cotransporter; renal outer medulla K^+ channel; hyperprostaglandin E syndrome

HYPERPROSTAGLANDIN E SYNDROME (HPS) represents a genetically heterogeneous group of hypokalemic renal salt-wasting tubulopathies characterized by metabolic alkalosis, normotensive hyperaldosteronism, and increased renin and PGE_2 production (3, 29–31, 34). All HPS subtypes are linked to dysfunction of salt transport in the thick ascending limb (TAL) (12). Salt absorption by the Na^+-K^+-$2Cl^-$ cotransporter (NKCC2) in the TAL depends on the luminal availability of potassium which is recycled across the apical membrane by K^+ channels formed or dependent on ROMK expression (10, 11). Thus loss-of-function mutations in the ROMK (*Kcnj1*) result in HPS (type II Bartter's syndrome). In a companion paper, we characterized the renal phenotype of the ROMK null ($Romk^{-/-}$) mouse model of type II Bartter's syndrome based on the effects of specific loop of Henle and distal tubule diuretics on renal water and electrolyte excretion (4).

Impaired Na^+ transport in the TAL leads to enhanced downstream Na^+ delivery to the DCT, connecting tubule (CNT), and cortical collecting duct (CCD) (for a review, see Refs. 16, 18, and 25). Previous studies in rats have shown that chronic inhibition of sodium absorption in the TAL by loop diuretics like furosemide causes hypertrophy and hyperplasia of the DCT, CNT, and CCD associated with an increased abundance of the apical Na^+-Cl^- cotransporter (NCC), epithelial Na^+ channel (ENaC), and basolateral Na^+-K^+-ATPase (1, 9, 14, 17, 24, 28). These adaptive mechanisms have been suggested to play a role in the development of furosemide resistance that occurs frequently during treatment with loop diuretics (25). Similar functional adaptations of the distal nephron could help compensate for derangements of function of the loop of Henle in HPS. Thus, in the present study, we examined the adaptive responses in ion transport proteins along the nephron in the ROMK null mouse model of type II Bartter's syndrome.

MATERIALS AND METHODS

Mice. The generation of $Romk^{+/+}$ and $Romk^{-/-}$ mice has been previously described (21; see also Ref. 4). Survival of $Romk^{-/-}$ mice to adults was >50%. Wild-type $Romk^{+/+}$ are genetically identical to $Romk^{-/-}$ mice except for deletion of *Kcnj1*. All mice were given tap water ad libitum and maintained on standard rodent chow (1.2% K). All animal experiments were approved by the Yale Animal Care Committee.

Urine collection. Mice were housed in metabolic cages with free access to normal food and water. Urine samples were collected over 16 h into tubes immersed in ice during collection.

* C. A. Wagner and D. Loffing-Cueni contributed equally to this work.

Addresses for reprint requests and other correspondence: C. A Wagner, Institute of Physiology, Center for Integrative Human Physiology, Univ. of Zurich, Winterthurerstrasse 190, CH-8057 Zurich, Switzerland (e-mail: Wagnerca@access.uzh.ch) and J. Loffing, Institute of Anatomy, Univ. of Zurich, Winterthurerstrasse 190, CH-8057 Zurich, Switzerland (e-mail: johannes.loffing@anatom.uzh.ch).

Serum PGE_2 and aldosterone measurements. PGE_2 concentrations were determined by using a PGE_2 EIA Kit (Cayman Chemical, Ann Arbor, MI) according to the manufacturer's instructions. Briefly, after dilution of urine samples to the optional concentration, 50 μl of each sample was mixed along with a serial dilution of PGE_2 standard samples with appropriate amounts of acetylcholinesterase-labeled tracer and PGE_2 antiserum and incubated at 4°C for 18 h. After the wells were emptied and rinsed with wash buffer, 200 μl of Ellman's reagent containing the acetylcholinesterase substrate was added. The enzyme reaction was carried out on a slow shaker at room temperature for 1–2 h. The plates were read on a Microplate Reader (Benchmark Microplate Reader, Bio-Rad) at 405 nm. The results were analyzed with Cayman Chemical's computer spreadsheet.

Plasma aldosterone concentrations were measured in blood samples collected from the carotid artery using an Immuchem Double Antibody, Aldosterone ^{125}I RIA kit at Yale University's General Clinical Research Center. The RIA kit was purchased from ICN Pharmaceuticals (Costa Mesa, CA).

Antibodies. The antibodies used for immunohistochemistry and Western blotting are shown in Table 1.

The new sets of antibodies against NKCC2, β-ENaC, γ-ENaC, and aquaporin-2 (AQP2), were obtained by immunizing rabbits (Pineda Ab-Production, Berlin, Germany) with keyhole limpet hemocyanin-coupled synthetic peptides corresponding to amino acid sequences within mouse NKCC2 (NH_2-CEYYRNTGSVSGPKVNRPSLQE-COOH), β-ENaC (NH_2-CNYDSLRLQPLDTMESDSEVEAI-COOH), γ-ENaC (NH_2-CNTLRLDSAFSSQLTDTQLTNEF-COOH), or AQP2 (NH_2-CVELHSPQSLPRGSKA-COOH), similar to previously used sequences of rat or human isoforms of these proteins (7, 8, 22).

All sera were characterized by immunofluorescence and standard Western blotting with mouse kidney samples. Specific binding of the antibodies to kidney sections (immunofluorescence) and to polyvinylidene difluoride (PVDF) membranes (Western blotting) could be completely inhibited by preincubation of the antisera with the specific peptides used for immunization (see supplementary figures; all supplementary material is available in the online version of this article at the journal web site).

Western blotting. The mice were killed, and the kidneys were rapidly harvested. Total kidneys were homogenized in an ice-cold K-HEPES buffer (200 mM mannitol, 80 mM K-HEPES, 41 mM KOH, pH 7.5) with pepstatin, leupeptin, K-EDTA, and phenylmethylsulfonyl fluoride (PMSF) added as protease inhibitors. The samples were centrifuged at 1,000 *g* for 10 min at 4°C, and the supernatant was saved. Subsequently, the supernatant was centrifuged at 100,000 *g* for 1 h at 4°C, and the resultant pellet was resuspended in K-HEPES buffer containing protease inhibitors. After measurement of the total protein concentration (Bio-Rad Protein kit), 50 μg of crude membrane protein were solubilized in Laemmli sample buffer, and SDS-PAGE was performed on 10% polyacrylamide gels. For immunoblotting, proteins were transferred electrophoretically from unstained gels to PVDF membranes (Immobilon-P, Millipore, Bedford, MA). After blocking with 5% milk powder in Tris-buffered saline/0.1% Tween 20 for 60 min, the blots were incubated with the primary antibody either for 2 h at room temperature or overnight at 4°C. After washing and subsequent blocking, blots were incubated with the secondary antibodies (donkey anti-rabbit 1:10,000 and sheep anti-mouse 1:5,000, IgG conjugated with horseradish peroxidase, Amersham Life Sciences) for 1 h at room temperature. Antibody binding was detected with an enhanced chemiluminescence ECL kit (Amersham Pharmacia Biotech) before exposure to X-ray film (Kodak). The protein/actin ratio was determined and used to calculate the ratio between the wild-type and ROMK-deficient group using Gauss' law of error propagation. All results were tested for significance using the unpaired Student's *t*-test, and only results with $P < 0.05$ were considered as statistically significant.

Western blot analysis of renin expression. Mouse kidneys were homogenized in 1–2 ml of extraction buffer (5 mM Tris hydrochloride, pH 7.5, 2 mM EDTA, 1% SDS, 100 μM PMSF, 2 μg/ml leupeptin, and 2 μg/ml aprotinin), and centrifuged at 4,000 *g* for 30 min at 4°C. Protein concentration was determined using a BCA Protein assay kit (Pierce, Rockford, IL). Forty micrograms of protein was solubilized in 2× sample buffer, separated by 10% SDS-PAGE, and transferred to PVDF membranes using the Mini-Trans blotting system (Bio-Rad Laboratories, Hercules, CA). Prestained high-range SDS-PAGE standards were used (Bio-Rad Laboratories). The membranes were blocked for 1 h in 5% nonfat milk/TBS-Tween at room temperature before incubation with the primary mouse monoclonal anti-renin antibody (Research Diagnostics) diluted 1:1,000 in 5% nonfat milk/TBS-Tween overnight at 4°C. After washing, membranes were incubated with peroxidase-linked anti-mouse IgG antibodies (Amersham Life Science, Arlington Heights, IL) for 1 h at room temperature. After washing in TBS-Tween, antigen-antibody complexes were detected using the ECL chemiluminescence kit (ECL, Amersham Life Science).

Immunohistochemistry. Mice were anesthetized with ketamine/xylazine (ip). and perfused through the left ventricle with PBS followed by paraformaldehyde-lysine-periodate fixative (23). Immunohistochemistry was performed as previously described (20). Briefly, cryosections 5 μm thick were incubated overnight at 4°C with antibodies given in Table 1. Binding sites were revealed by Cy3-conjugated goat anti-rabbit IgG antibodies. Sections were studied by epifluorescence on a Zeiss microscope. Histological and morpho-

Table 1. *Antibodies used for immunohistochemistry and Western blotting*

Antibody	Host	Dilution		Source	Reference
		WB	IF		
NHE3	Rabbit	1:5,000		O. Moe	2
NaPi-IIa	Rabbit	1:5,000		H. Murer	5
NKCC2	Rabbit	1:5,000		S. Hebert	15
		1:20,000	1:20,000	J. Loffing	This study
ROMK	Rabbit	1:500	1:500	Alamone	
NCC	Rabbit	1:2,000	1:2,000	J. Loffing	20
AQP2	Rabbit	1:20,000	1:20,000	J. Loffing	This study
α−ENaC	Rabbit	1:2,000	1:500	B. Rossier	27
β−ENaC	Rabbit		1:500	B. Rossier	27
		1:20,000	1:20,000	J. Loffing	This study
γ−ENaC	Rabbit		1:400	B. Rossier	27
		1:20,000	1:20,000	J. Loffing	This study
β-Actin	Mouse	1:5,000		Sigma	

WB, Western blotting; IF, immunofluorescence; isoform 3 Na^+/H^+ exchanger; type IIa Na^+-P_i cotransporter; NKCC2, Na^+-K^+-$2Cl^-$ cotransporter; NCC, Na^+- Cl^- cotransporter; AQP2, aquaporin-2; ENaC, epithelial Na^+ channel.

metrical analysis was performed by two experienced investigators blinded for the genotype of the animals. Digital images were taken with a charge-coupled device camera.

Quantification of α-ENaC by real-time PCR. ROMK wild-type and knockout mice were killed by injection of ketamine/xylazine (ip) and subsequent cervical dislocation, and the kidneys were collected and rapidly frozen until further use. Total mRNA was extracted from 30 mg of tissue using an RNA Aqueous 4PCR kit (Ambion) according to the manufacturer's instruction. For RNA extraction, kidneys was thawed in RNALater solution (Ambion), transferred to lysis buffer, and homogenized on ice with an Elvehjem potter. RNA was bound on columns and treated with DNAse for 15 min at 30°C to reduce genomic DNA contamination. Quantity and purity of total eluted RNA were assessed by spectrometry and on agarose gels. Each RNA sample was diluted to 200 ng/μl, and 3 μl was used as a template for reverse transcription using a Taqman Reverse Transcription kit (Applied Biosystems) in the presence of 2.5 μM Random Hexamers primers (Applied Biosystems).

For reverse transcription, a 200-ng RNA template was diluted in a 20-μl reaction mix that contained (final concentrations) RT buffer (1×), $MgCl_2$ (5.5 mM), random hexamers (2.5 μM), RNAse inhibitor (0.4 U/μl), the multiscribe RT enzyme (1.25 U/μl), deoxyNTP mix (500 μM each), and RNAse-free water. Real-time PCR was performed as described previously, according to the recommendations supplied by Applied Biosystems (http://home.appliedbiosystems.com). Primers for all genes of interest were designed using Primer Express 2.0 software from Applied Biosystems. Primers were chosen to result in amplicons of 70–100 bp that span intron-exon boundaries. The specificity of all primers was first tested on mRNA derived from kidneys and resulted in a single product of the expected size (data not shown). Probes were labeled with the reporter dye FAM at the 5′-end and the quencher dye TAMRA at the 3′-end (Microsynth, Balgach, Switzerland). The passive reference dye (ROX) was included in the Taqman buffer supplied by the manufacturer. Twenty microliters of cDNA obtained from the RT reaction was diluted to 100 μl with RNAse-free water. A 25-μl PCR reaction volume was prepared using 5 μl diluted cDNA as a template with sense and antisense primers (25 μM each) and the labeled probe (5 μM). The sequences for primers used were the following: β-actin forward primer: 5′-CCACCGATCCACACAGAGTACTT-3′, β-actin reverse primer: 5′-GACAGGATGCAGAAGGAGATTACTG-3′; and α-ENaC forward primer: 5′-GGTGCACGGTCAGGATGAG-3′, α-ENaC reverse primer: 5′-TAGTTGCCTCCGAGGCTGTC-3′. The Taqman Universal PCR Master Mix (Applied Biosystems) was added to the final volume. Reactions were run in 96-well optical reaction plates using a Prism 7700 cycler (Applied Biosystems).

Thermal cycles were set at 95°C (10 min) and the 40 cycles at 95 (15 s) and 60°C (1 min) with auto-ramp time. To analyze the data, the threshold was set to 0.06 (value in the linear range of amplification curves). All the reactions were run in triplicate. The abundance of α-ENaC mRNA was calculated relative to a reference mRNA (mouse β-actin). Assuming an efficiency value of 2 (fold-increase in input mRNA required to decrease the cycle number by 1), relative expression ratios were calculated as

$$R = 2^{(C_t(\beta\text{-actin}) - C_t(\alpha\text{-ENaC}))}$$

where C_t is the cycle number at the threshold.

In situ microperfusion of mouse kidney proximal tubules. The net fluid and HCO_3^- absorption in proximal tubules of age-matched adult ROMK null and wild-type mice was assessed by in situ microperfusion as described previously (32). Briefly, superficial proximal convoluted tubules were perfused at a rate of 15 nl/min with a solution containing 115 mM NaCl, 25 mM $NaHCO_3$, 4 mM KCl, 2 mM $CaCl_2$, 1 mM $MgSO_4$, 2 mM $NaPO_4$, and 20 μCi/ml low-Na^+ methoxy-[^{3}H]inulin (pH 7.4). The rates of net fluid (J_v) and HCO_3^- (J_{HCO3}) absorption were calculated based on changes in the concentrations of [^{3}H]inulin and total CO_2 as described previously (33). J_v and J_{HCO3} are expressed per minute per millimeter of proximal tubule.

RESULTS

Hormone levels. HPS is associated with increased urinary excretion of PGE_2 (12). Measurement of urinary PGE_2 excretion in ROMK null mice demonstrated a nonsignificant 1.5-fold increase in PGE_2 levels in (PGE_2 wild-type: 1,099.9 ± 107.3 pg/day; *Romk*$^{-/-}$: 15,743.0 ± 209.2 pg/ day, $n = 12$, $P = 0.056$). Plasma aldosterone was slightly but significantly higher in *Romk*$^{-/-}$ animals than in *Romk*$^{+/+}$ mice (260.3 ± 31.0 vs. 181.5 ± 11.5 pg/ml, $P < 0.05$). In agreement with previous reports (12, 26) on enhanced plasma renin activity in patients with Bartter's syndrome, we found by Western blotting and immunohistochemistry increased renin abundance in kidneys from *Romk*$^{-/-}$ mice (data not shown).

Changes in proximal tubule salt and water transport proteins and transport rates in Romk$^{-/-}$ *mice.* Figure 1 shows the absence of ROMK expression in kidneys of *Romk*$^{-/-}$ mice by Western blotting of total crude membranes (Fig. 1*A*) and

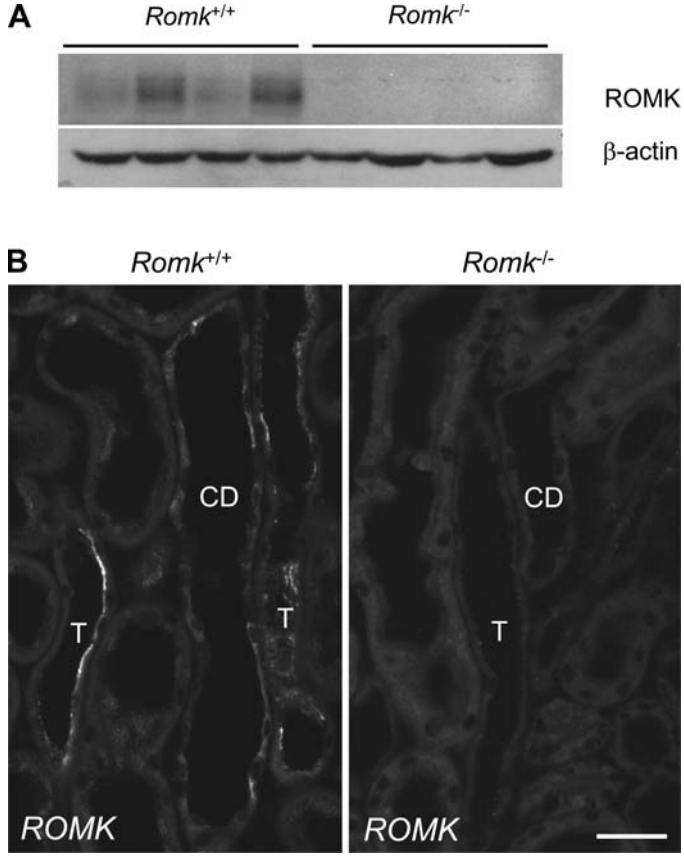

Fig. 1. Absence of ROMK from kidneys from ROMK-deficient mice (*Romk*$^{-/-}$). *A*: semiquantitative immunoblotting with homogenates from total kidneys of wild-type (*Romk*$^{+/+}$) and *Romk*$^{-/-}$ mice. Fifty micrograms of crude membrane preparations from each mouse were subjected to SDS-PAGE and transferred to polyvinylidene difluoride (PVDF) membrane and probed with affinity-purified anti-ROMK antibodies (Alamone Laboratories) and reprobed for β-actin after being stripped to control for loading. *B*: medullary rays in renal cortex of *Romk*$^{+/+}$ and *Romk*$^{-/-}$ mice. Immunostaining for ROMK with affinity-purified rabbit-anti-ROMK antibody shows prominent ROMK staining in the luminal membrane of some thick ascending limb (T) cells and in the cytoplasm of some collecting duct (CD) cells that is absent from kidneys of ROMK-deficient mice. Scale bar = ~50 μm.

immunofluorescence staining of tissue sections (Fig. 1*B*). The abundance of the proximal tubule Na^+-transport proteins Na^+/H^+ exchanger isoform 3 (NHE3) and Na^+-phosphate cotransporter type IIa (NaPi-IIa) was reduced by 10 ± 6 and 37 ± 12%, respectively (Fig. 2) in kidneys of *Romk*$^{-/-}$ mice compared with those of wild-type mice. This reduction may reflect the relative decrease in proximal tubular mass due to the increased fractional cortical tubular volume of distal convoluted tubules as described below. However, this 10% reduction of NHE3 expression in kidneys of *Romk*$^{-/-}$ mice did not significantly influence net Na^+ and HCO_3^- absorption in proximal tubules. As show in Fig. 3, J_v and J_{HCO3} absorption were not significantly different between *Romk*$^{+/+}$ and *Romk*$^{-/-}$ mice. Although the glomerular filtration rate in *Romk*$^{-/-}$ mice was ~50% of control *Romk*$^{+/+}$ mice (4), the single-nephron glomerular filtration rate was not reduced in *Romk*$^{-/-}$ mice (21). Since NHE3 activity is flow dependent (6), the 10% reduction of NHE3 expression was not detectable by changes in J_v and J_{HCO3} absorption at the flow rate close to the normal single-nephron glomerular filtration rate in the proximal tubule.

Changes in loop and distal tubule salt and water transport proteins in Romk$^{-/-}$ *mice.* NaCl absorption in the loop of Henle is markedly reduced but not absent in *Romk*$^{-/-}$ mice (21), and these ROMK null mice exhibit a small remaining responsiveness to loop diuretics (4). Thus we assessed the abundance of the TAL-specific apical NKCC2 isoform in *Romk*$^{-/-}$ mice. In the absence of ROMK expression, NKCC2 was decreased in *Romk*$^{-/-}$ mice by 42 ± 16% (Fig. 4*A*). With the use of the same antibody, immunofluorescence revealed NKCC2 in TAL segments of ROMK-deficient mice (Fig. 4*B*). The staining, however, was less prominent than in TAL segments of wild-type mice. The epithelial structure of the TAL segments of both genotypes was similar.

In a companion study (4), we showed that the natriuretic response to hydrochlorothiazide was exaggerated in *Romk*$^{-/-}$ mice. Thus we assessed the expression of the DCT-specific NCC and morphology of the DCT in *Romk*$^{-/-}$ compared with *Romk*$^{+/+}$ mice. NCC abundance was markedly enhanced in *Romk*$^{-/-}$ mice by 130 ± 36% (Fig. 5*A*). Overviews of renal cortex in wild-type and *Romk*$^{-/-}$ mice showed an increased abundance of nephron segments positive for NCC (Fig. 5, *B* and *C*). Higher magnifications revealed a pronounced epithelial hypertrophy of NCC-positive DCT profiles in ROMK-deficient mice (Fig. 5, *D* and *E*). Fractional DCT tubular volume in the cortex was more than threefold greater in *Romk*$^{-/-}$ compared with *Romk*$^{+/+}$mice (Fig. 5*F*). Interestingly, coimmunostainings for NCC and ENaC for unequivocal identification of mouse DCT subsegments (16) showed that DCT hypertrophy occurred predominately in the early rather then in the late DCT segments. (Fig. 6, *E* and *F*). In the companion study (4), we found that benzamil, an inhibitor of ENaC, did not increase natriuresis in *Romk*$^{-/-}$ mice, suggesting that ENaC activation does not significantly contribute to the compensation of the Na^+ transport defect in the TAL. Consistent with this assumption, we found that plasma aldosterone levels were only slightly elevated and that the renal mRNA expression of the aldosterone-dependent α-ENaC subunit was not changed in *Romk*$^{-/-}$ mice (Fig. 6*B*). Although immunoblotting of whole kidney homogenates (Fig. 6*A*) revealed an increased abundance for α-ENaC by 345 ± 85% (not significant), β-ENaC by 203 ± 73% (not significant), and γ-ENaC by 197 ± 13% ($P < 0.05$), detailed immunohistochemical analysis of fixed kidney samples showed that the enhanced expression of ENaC subunits did not increase the cell surface abundance of ENaC. In mice of both genotypes, β-ENaC and γ-ENaC subunits were seen diffusely distributed in the cytoplasm of the segment-specific cells of the CNT and CCD (Fig. 6, *D*, *F–H*). Only

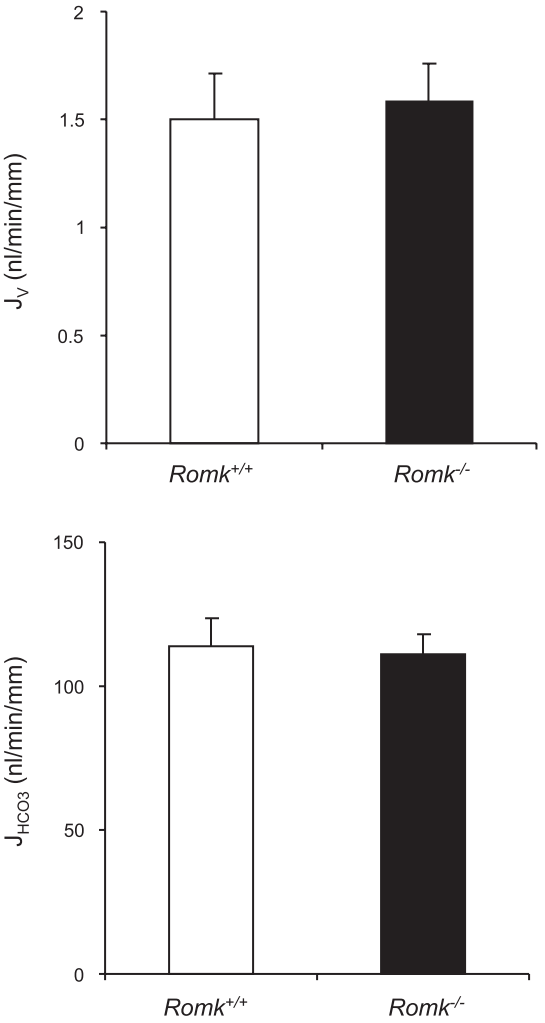

Fig. 3. Fluid and bicarbonate absorption in kidney proximal tubules The net fluid (J_v) and bicarbonate (J_{HCO3}) absorption were measured by microperfusion of proximal tubules in situ in both *Romk*$^{+/+}$ and *Romk*$^{-/-}$ mice.

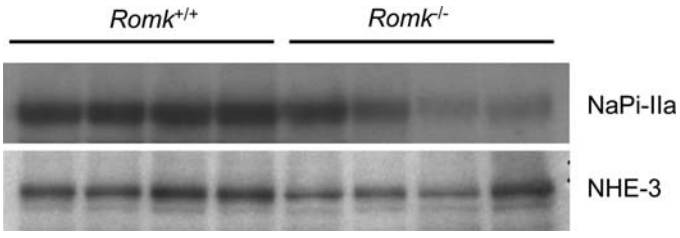

Fig. 2. Altered abundance of proximal tubular transport proteins in ROMK-deficient mice. Semiquantitative immunoblotting was performed with 50 μg of crude membrane preparations from *Romk*$^{+/+}$ and *Romk*$^{-/-}$ mouse kidneys. Compared with wild-type mice, ROMK-deficient mice exhibit reduced renal abundance of Na^+-P_i cotransporter type IIa (NaPi-IIa) and Na^+/H^+ exchanger isoform 3 (NHE3).

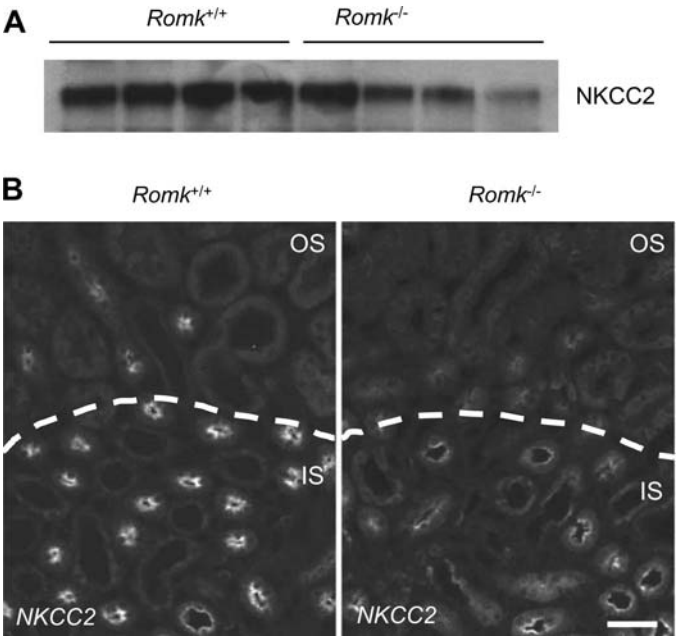

Fig. 4. Reduced abundance and immunostaining for the thick ascending limb of Henle's loop (TAL)-specific Na^+-K^+-$2Cl^-$ cotransporter (NKCC2/BSC1). *A*: semiquantitative immunoblotting with 50 μg of crude membrane preparations from $Romk^{+/+}$ and $Romk^{-/-}$ mouse kidneys. ROMK-deficient mice showed reduced abundance of the TAL-specific NKCC2. *B*: outer and inner stripe (OS and IS, respectively) of renal outer medulla of $Romk^{+/+}$ and $Romk^{-/-}$ mice. Immunostaining for NKCC2 is seen in the luminal membrane of TAL in wild-type and ROMK-deficient mice. The epithelial cells of TALs in ROMK-deficient mice do not show any gross abnormalities but apparently reveal weaker NKCC2 immunofluorescence than the TALs of wild-type mice. Scale bar = ~50 μm.

the late DCT and the initial portion of the CNT of $Romk^{-/-}$ mice revealed some staining for β-ENaC (Fig. 6*F*) and γ-ENaC (not shown) at the apical plasma membrane, similar to wild-type mice in this study (Fig. 6*D*) and similar to previous findings in normal mice and rats (16, 18, 19). α-ENaC was barely detectable by immunofluorescence in all segments of the CNT and collecting system in kidneys from wild-type and ROMK-deficient animals (data not shown).

Although there was variable expression of the AQP2 water channel in both $Romk^{-/-}$ and $Romk^{+/+}$ mice, the abundance of AQP2 was unchanged in $Romk^{-/-}$ mice (Fig.. 7*A*). AQP2 water channel staining appeared to be more luminal and pronounced in the CNT and CCD of some but not all ROMK-deficient mice compared with wild-type animals, suggesting broad interindividual variability (Fig. 7, *B–D*).

DISCUSSION

The antenatal Bartter's syndromes present clinically as TAL tubulopathies with a variable degree of salt and water loss depending on the underlying gene defect (3, 10, 12, 29–31, 34). Previous work using loop diuretic-treated rats and mice demonstrated an adaptive remodeling of the distal nephron with compensatory growth and upregulation of NaCl-absorbing proteins (9, 14). Similarly, inhibition of salt absorption in the distal nephron as with thiazide treatment or after genetic ablation of the NCC results in the compensatory hypertrophy of the CNT and CCD segments (20). ROMK channel-deficient mice provide a genetic model with which to study the possible

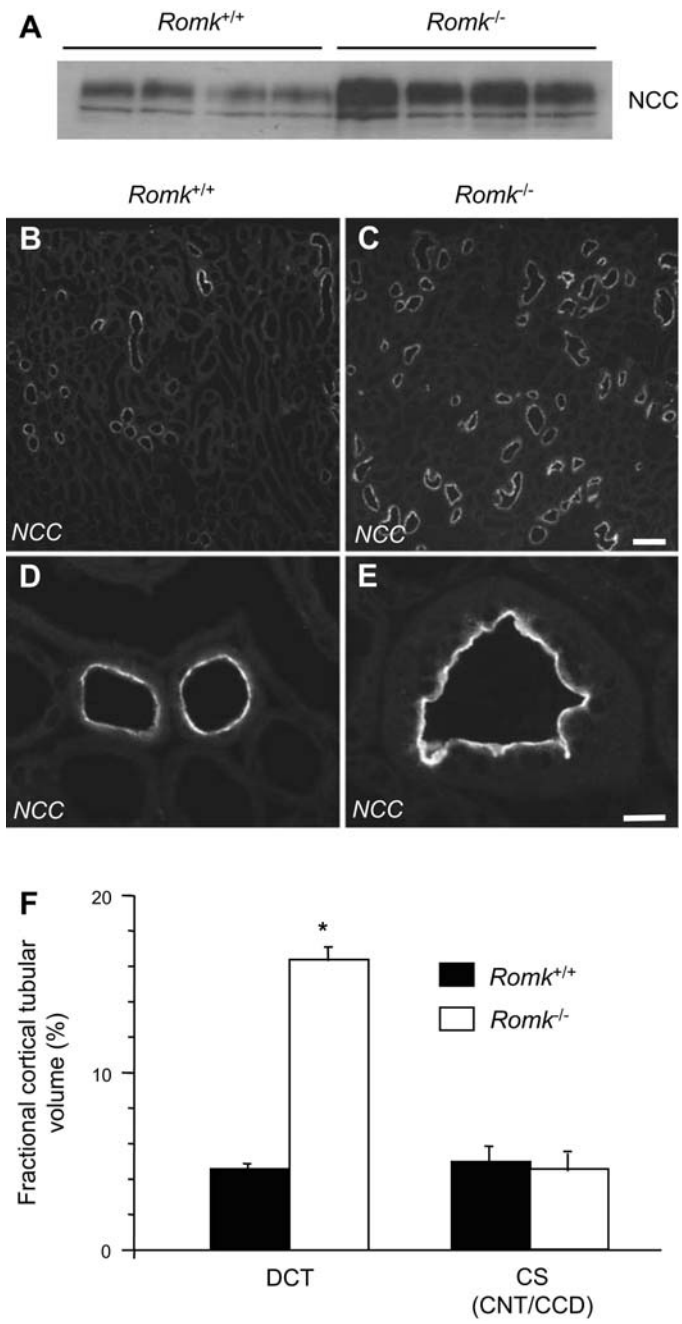

Fig. 5. Compensatory increased abundance in the thiazide-sensitive Na^+-Cl^- cotransporter (NCC) and massive hypertrophy of the distal tubule in kidneys from ROMK-deficient mice. *A*: semiquantitative immunoblotting with 50 μg of crude membrane preparations from $Romk^{+/+}$ and $Romk^{-/-}$ mouse kidneys. ROMK-deficient mice showed increased abundance of distal convoluted tubule (DCT)-specific NCC. *B* and *C*: overviews of renal cortex of $Romk^{+/+}$ and $Romk^{-/-}$ mice. Immunofluorescence with rabbit anti-NCC antibodies reveals much higher density of NCC-positive DCT profiles in the renal cortex of the $Romk^{-/-}$ mouse than in the renal cortex of the $Romk^{+/+}$ mouse. Scale bar = ~200 μm. *D* and *E*: higher magnification of NCC-immunostained DCT profiles demonstrates the tremendous hypertrophy of the DCT epithelium in ROMK-deficient mice. Pictures were taken at the same magnification. Scale bar = ~20 μm. *F*: fractional cortical volumes of DCT and the cortical collecting system [connecting tubule (CNT) and cortical collecting duct (CCD)] in $Romk^{+/+}$ and $Romk^{-/-}$ mice. DCT and CNT/CCD were identified on account of their characteristic antibody-binding [DCT: NCC positive; CNT/CCD: NCC negative; and β-epithelial sodium channel (ENaC) positive] as described in MATERIALS AND METHODS. The fractional cortical tubular volumes were determined by the point-counting method, according to Weibel (35). Values are means ± SE from 4 individual mice in each group. *$P < 0.05$ vs. $Romk^{-/-}$ values.

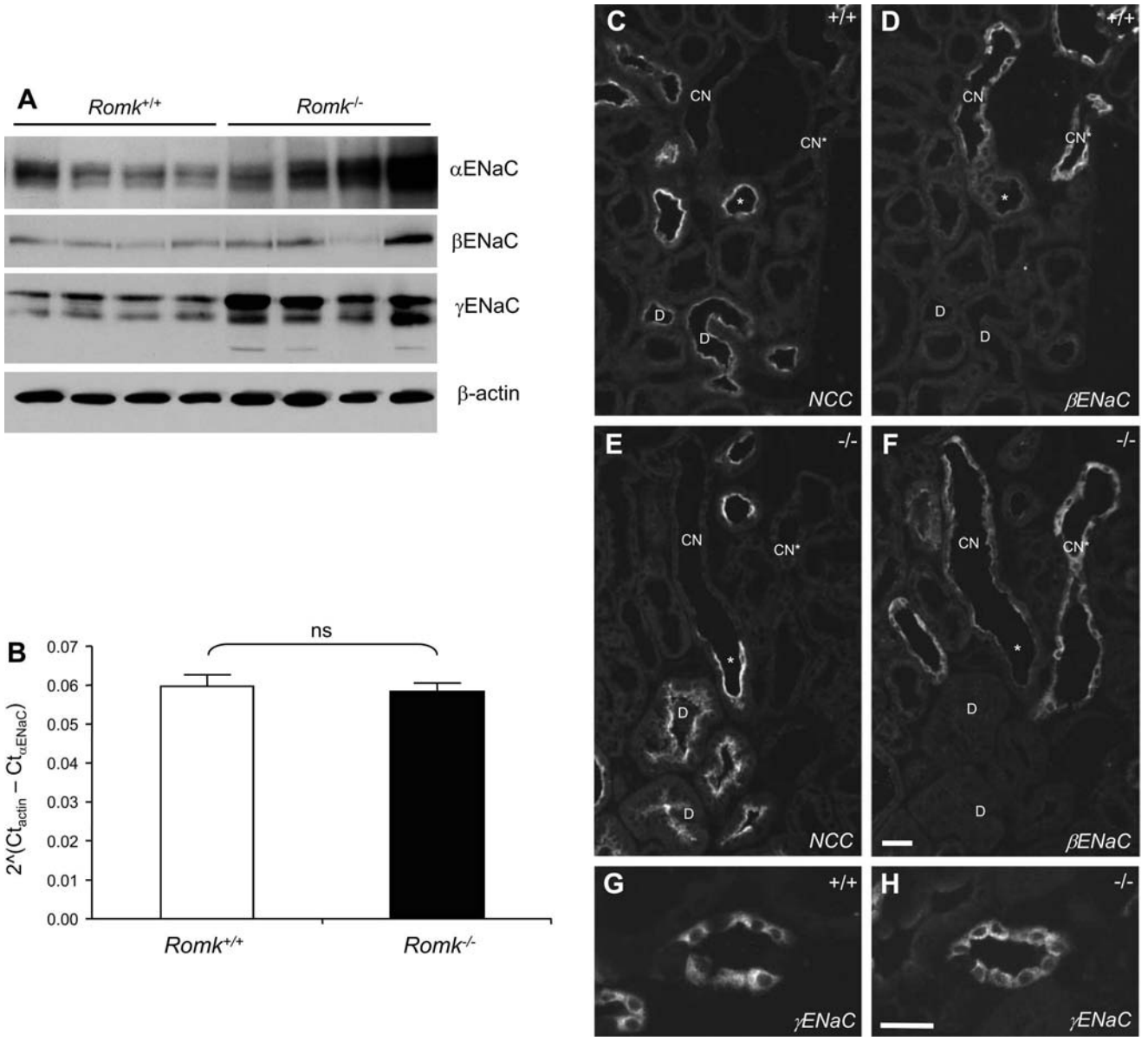

Fig. 6. Abundance and localization of ENaC subunits. *A*: semiquantitative immunoblotting with 50 μg of total membrane preparations from kidneys of $Romk^{+/+}$ and $Romk^{-/-}$ mice. The abundance of the α-ENaC and γ-ENaC subunits is profoundly increased, whereas the expression of β-ENaC appears to be unaffected. Polyvinylidene difluoride (PVDF) membranes were stripped and reprobed for β-actin to ensure equal loading. *B*: relative abundance of mRNA for the aldosterone-regulated α-ENaC as determined by real-time PCR and normalized against β-actin mRNA. *C–F*: consecutive cryosections of renal cortex of $Romk^{+/+}$ (*C* and *D*) and $Romk^{-/-}$ (*E* and *F*) mice immunostained for NCC (*C* and *E*) and β-ENaC (*D* and *F*). Note the marked hypertrophy of early DCT (*D*) profiles, (characterized by strong NCC, but no β-ENaC immunoreactivity) in $Romk^{-/-}$ mice compared with early DCTs of $Romk^{+/+}$ mice. The epithelial heights of late DCT profiles (asterisks), which are characterized by costaining for NCC and β-ENaC, and of CNT profiles (CN) do not apparently vary between the two mice. Similarly, mice of both genotypes show apical β-ENaC immunostaining only in the late DCT (asterisk) and in the directly adjacent early connecting tubule (CN). In farther downstream localized CNT (CN*) segments, β-ENaC is almost exclusively localized to intracellular compartments in mice of both genotypes. Scale bar = ~40 μm. *G* and *H*: higher magnification of CNT profiles from $Romk^{+/+}$ and $Romk^{-/-}$ mice demonstrate the predominant intracellular localization of γ-ENaC in the CNTs from mice of both genotypes. Unstained cells in the CNT epithelia represent intercalated cells, which are known to be ENaC negative. Scale bar = ~40 μm.

compensatory mechanisms involved in this type II Bartter's disease. We show that loss of ROMK is associated with reduced expression of proximal tubular and TAL Na^+ transporters, DCT cell hypertrophy with increased DCT NCC abundance, and slightly enhanced abundance of ENaC Na^+ channels in the collecting system, which are, however, predominantly localized to intracellular compartments.

These results are in agreement with functional data obtained in the same animals, as described in the companion study (4). The reduction of NKCC2 expression and a reduced effect of furosemide on the fractional Na^+ excretion rate together demonstrate that ROMK is critical for TAL function. The absence of apparent structural changes in the TAL is consistent with previous morphological studies using kidneys of furosemide-treated rats (12, 13). Moreover, it appears that most of the lost TAL function is compensated for by the subsequent distal tubule as indicated by the massive hypertrophy of the DCT epithelium, the increase in the expression levels of the thiazide-

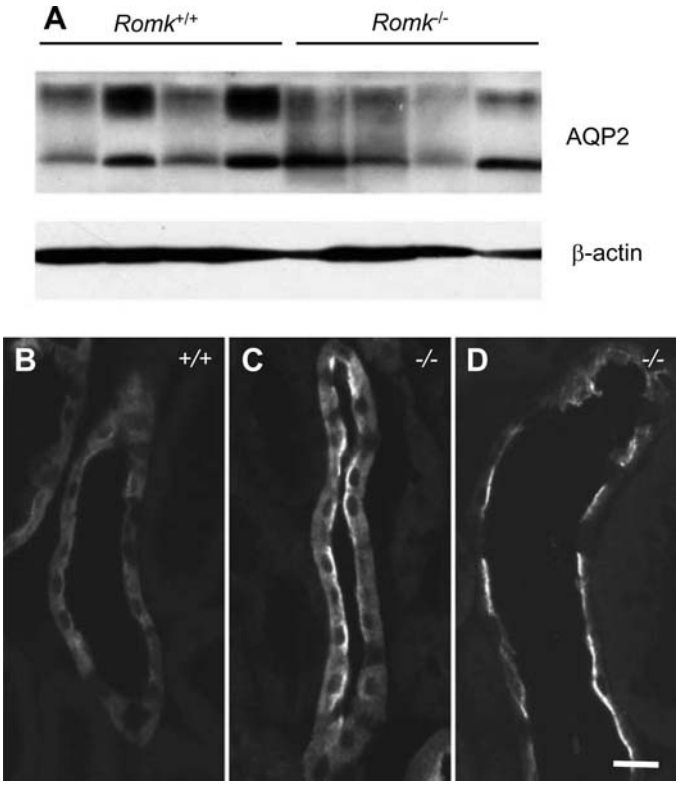

Fig. 7. Expression and localization of the vasopressin-regulated aquaporin-2 (AQP2) water channel. *A*: semiquantitative immunoblotting for AQP2 with total membrane preparations from total kidney of $Romk^{+/+}$ and $Romk^{-/-}$ animals reveals no significant difference between both genotypes. *B–D*: medullary rays in renal cortex of $Romk^{+/+}$ and $Romk^{-/-}$ mice. Immunostaining for AQP2 with affinity-purified rabbit anti-AQP2 antibody. *B*: AQP2 immunofluorescence is visible in the luminal membrane and in the cytoplasm of collecting duct principal cells. Intercalated cells are AQP2 negative. The collecting ducts of ROMK-deficient mice often exhibit more pronounced intracellular and apical AQP2 immunostaining (*C*). In some collecting duct profiles of ROMK-deficient mice (*D*), AQP2 is almost exclusively localized at the apical plasma membrane. Scale bar = ~20 μm.

sensitive NaCl-cotransporter NCC, and the exaggerated response in urinary Na^+ excretion after application of thiazide diuretics. The fractional cortical tubular volume of the DCT increased >300%, which readily explains the previously reported higher volume density of distal tubules in $Romk^{-/-}$ mice (21). The structural changes in the DCT are reminiscent of those seen in furosemide-treated rats. In these rats, the pharmacological inhibition of TAL function also induced DCT cell growth (13, 14), which was, however, less dramatic as that seen in $Romk^{-/-}$ mice. Although not specifically addressed in the present study, results from furosemide-treated rats indicate that the observed adaptive DCT growth originates from both epithelial hypertrophy (9, 14) and epithelial hyperplasia (17). PGE_2 has been implicated in the hypertrophy of distal nephron segments but has also been made responsible, at least in part, for the pathophysiology observed in Bartter's syndrome (12). Hence, it remains to be clarified whether PGE_2 is part of the compensatory response or rather contributes to the observed renal defect. ROMK-deficient mice will provide an excellent model for the study of this problem in the future.

Although $Romk^{-/-}$ mice have a severe Na^+-transporting defect in the TAL, the animals are apparently more or less in sodium balance, as indicated by the only slightly elevated plasma renin and aldosterone levels. Consistent with the rather minor effect on plasma aldosterone levels, $Romk^{-/-}$ mice did not show any significant upregulation of the aldosterone-dependent α-ENaC subunit at the mRNA level and no effect on the cell surface localization of all three ENaC subunits. Similarly, the renal clearance experiments (see Ref. 4, the companion study) did not show any significant difference between the amiloride-sensitive portion of renal Na^+ reabsorption in wild-type and ROMK-deficient mice. Together with the lack of any effect on the fractional cortical tubular volume of the collecting system, these data strongly suggest that ENaC-mediated Na^+ transport in the collecting system is not significantly activated and therefore does not significantly contribute to the compensation of the renal Na^+ transport defect in ROMK-deficient mice. This stands in sharp contrast to the compensatory mechanisms in NCC-deficient mice. These mice revealed elevated plasma aldosterone levels, increased ENaC cell surface abundance, and a marked epithelial hypertrophy of the renal connecting tubule but not of the collecting duct (20). Taken together, these findings suggest that the genetic salt transport defect in a given distal tubular segment is largely compensated by structural and functional adaptations in the directly following downstream tubular segment. Consistent with this hypothesis is our observation in the present study that the DCT hypertrophy in $Romk^{-/-}$ mice is most pronounced in the early DCT.

Interestingly, no clear effect was found in AQP2 water channels. Despite the fact that $Romk^{-/-}$ animals are polyuric and that some of them showed a more pronounced apical AQP2 staining with the appearance of AQP2 channels also in the CNT, this effect was not observed in all animals. Immunoblotting also showed no significant difference between wild-type and knockout animals.

In summary, ablation of ROMK channels in the TAL in the mouse kidney leads to loss of TAL function. Excessive water and salt loss are prevented by a combination of hypertrophy of the subsequent distal nephron and upregulation of NaCl reabsorption via the thiazide-sensitive NCC cotransporter and to a lesser extent via ENaC. Upregulation of AQP2 channels appears to play a minor role and was not observed in all animals. Thus the ROMK-deficient mouse model provides good evidence for compensatory mechanisms in Bartter's syndrome and TAL dysfunction and will allow study of the mechanism underlying these compensatory processes.

ACKNOWLEDGMENTS

We thank Drs. O. Moe, H. Murer, and B. Rossier for providing antibodies against NHE3, NaPi-IIa, and ENaC, respectively.

GRANTS

This study was supported by grants from the Swiss National Research Foundation to C. A. Wagner (31-109677/1) and J. Loffing (3200B0-105769), the EU 6th framework program EUREGENE to C. A. Wagner, a Marie Heim-Vögtlin fellowship and the Research Fund of the University of Fribourg to D. Loffing-Cueni, and National Institute of Diabetes and Digestive and Kidney Diseases Grants DK-54999 (to S. C. Hebert) and DK-62289 and DK-17433 (to T. Wang).

REFERENCES

1. **Abdallah JG, Schrier RW, Edelstein C, Jennings SD, Wyse B, Ellison DH.** Loop diuretic infusion increases thiazide-sensitive Na^+/Cl^--cotransporter abundance: role of aldosterone. *J Am Soc Nephrol* 12: 1335–1341, 2001.
2. **Amemiya M, Loffing J, Lotscher M, Kaissling B, Alpern RJ, Moe OW.** Expression of NHE-3 in the apical membrane of rat renal proximal tubule and thick ascending limb. *Kidney Int* 48: 1206–1215, 1995.
3. **Birkenhager R, Otto E, Schurmann MJ, Vollmer M, Ruf EM, Maier-Lutz I, Beekmann F, Fekete A, Omran H, Feldmann D, Milford DV, Jeck N, Konrad M, Landau D, Knoers NV, Antignac C, Sudbrak R, Kispert A, Hildebrandt F.** Mutation of BSND causes Bartter syndrome with sensorineural deafness and kidney failure. *Nat Genet* 29: 310–314, 2001.
4. **Cantone A, Yang X, Yan Q, Giebisch G, Hebert SC, Wang T.** Mouse model of type II Bartter's syndrome. I. Upregulation of thiazide-sensitive Na-Cl cotransport activity. *Am J Physiol Renal Physiol* (First published April 2, 2008). doi: 10.1152/ajprenal.00608.2007
5. **Custer M, Lötscher M, Biber J, Murer H, Kaissling B.** Expression of Na-P_i cotransport in rat kidney: localization by RT-PCR and immunohistochemistry. *Am J Physiol Renal Fluid Electrolyte Physiol* 266: F767–F774, 1994.
6. **Du Z, Yan Q, Duan Y, Weinbaum S, Weinstein AM, Wang T.** Axial flow modulates proximal tubule NHE3 and H-ATPase activities by changing microvillus bending moments. *Am J Physiol Renal Physiol* 290: F289–F296, 2006.
7. **Ecelbarger CA, Terris J, Hoyer JR, Nielsen S, Wade JB, Knepper MA.** Localization and regulation of the rat renal Na^+-K^+-$2Cl^-$ cotransporter, BSC-1. *Am J Physiol Renal Fluid Electrolyte Physiol* 271: F619–F628, 1996.
8. **Elliot S, Goldsmith P, Knepper M, Haughey M, Olson B.** Urinary excretion of aquaporin-2 in humans: a potential marker of collecting duct responsiveness to vasopressin. *J Am Soc Nephrol* 7: 403–409, 1996.
9. **Ellison DH, Velazquez H, Wright FS.** Adaptation of the distal convoluted tubule of the rat. Structural and functional effects of dietary salt intake and chronic diuretic infusion. *J Clin Invest* 83: 113–126, 1989.
10. **Hebert SC.** Bartter syndrome. *Curr Opin Nephrol Hypertens* 12: 527–532, 2003.
11. **Hebert SC.** Roles of Na-K-2Cl and Na-Cl cotransporters and ROMK potassium channels in urinary concentrating mechanism. *Am J Physiol Renal Physiol* 275: F325–F327, 1998.
12. **Jeck N, Schlingmann KP, Reinalter SC, Komhoff M, Peters M, Waldegger S, Seyberth HW.** Salt handling in the distal nephron: lessons learned from inherited human disorders. *Am J Physiol Regul Integr Comp Physiol* 288: R782–R795, 2005.
13. **Kaissling B, Bachmann S, Kriz W.** Structural adaptation of the distal convoluted tubule to prolonged furosemide treatment. *Am J Physiol Renal Fluid Electrolyte Physiol* 248: F374–F381, 1985.
14. **Kaissling B, Stanton BA.** Adaptation of distal tubule and collecting duct to increased sodium delivery. I. Ultrastructure. *Am J Physiol Renal Fluid Electrolyte Physiol* 255: F1256–F1268, 1988.
15. **Kaplan MR, Plotkin MD, Lee WS, Xu ZC, Lytton J, Hebert SC.** Apical localization of the Na-K-Cl cotransporter, rBSC1, on rat thick ascending limbs. *Kidney Int* 49: 40–47, 1996.
16. **Loffing J, Kaissling B.** Sodium and calcium transport pathways along the mammalian distal nephron: from rabbit to human. *Am J Physiol Renal Physiol* 284: F628–F643, 2003.
17. **Loffing J, Le Hir M, Kaissling B.** Modulation of salt transport rate affects DNA synthesis in vivo in rat renal tubules. *Kidney Int* 47: 1615–1623, 1995.
18. **Loffing J, Loffing-Cueni D, Valderrabano V, Klausli L, Hebert SC, Rossier BC, Hoenderop JG, Bindels RJ, Kaissling B.** Distribution of transcellular calcium and sodium transport pathways along mouse distal nephron. *Am J Physiol Renal Physiol* 281: F1021–F1027, 2001.
19. **Loffing J, Pietri L, Aregger F, Bloch-Faure M, Ziegler U, Meneton P, Rossier BC, Kaissling B.** Differential subcellular localization of ENaC subunits in mouse kidney in response to high- and low-Na diets. *Am J Physiol Renal Physiol* 279: F252–F258, 2000.
20. **Loffing J, Vallon V, Loffing-Cueni D, Aregger F, Richter K, Pietri L, Bloch-Faure M, Hoenderop JG, Shull GE, Meneton P, Kaissling B.** Altered renal distal tubule structure and renal Na^+ and Ca^{2+} handling in a mouse model for Gitelman's syndrome. *J Am Soc Nephrol* 15: 2276–2288, 2004.
21. **Lorenz JN, Baird NR, Judd LM, Noonan WT, Andringa A, Doetschman T, Manning PA, Liu LH, Miller ML, Shull GE.** Impaired renal NaCl absorption in mice lacking the ROMK potassium channel, a model for type II Bartter's syndrome. *J Biol Chem* 277: 37871–37880, 2002.
22. **Masilamani S, Kim GH, Mitchell C, Wade JB, Knepper MA.** Aldosterone-mediated regulation of ENaC alpha, beta, and gamma subunit proteins in rat kidney. *J Clin Invest* 104: R19–R23, 1999.
23. **McLean IW, Nakane PK.** Periodate-lysine-paraformaldehyde fixative. A new fixation for immunoelectron microscopy. *J Histochem Cytochem* 22: 1077–1083, 1974.
24. **Na KY, Oh YK, Han JS, Joo KW, Lee JS, Earm JH, Knepper MA, Kim GH.** Upregulation of Na^+ transporter abundances in response to chronic thiazide or loop diuretic treatment in rats. *Am J Physiol Renal Physiol* 284: F133–F143, 2003.
25. **Reilly RF, Ellison DH.** Mammalian distal tubule: physiology, pathophysiology, and molecular anatomy. *Physiol Rev* 80: 277–313, 2000.
26. **Reinalter SC, Jeck N, Brochhausen C, Watzer B, Nusing RM, Seyberth HW, Komhoff M.** Role of cyclooxygenase-2 in hyperprostaglandin E syndrome/antenatal Bartter syndrome. *Kidney Int* 62: 253–260, 2002.
27. **Rubera I, Loffing J, Palmer LG, Frindt G, Fowler-Jaeger N, Sauter D, Carroll T, McMahon A, Hummler E, Rossier BC.** Collecting duct-specific gene inactivation of alphaENaC in the mouse kidney does not impair sodium and potassium balance. *J Clin Invest* 112: 554–565, 2003.
28. **Scherzer P, Wald H, Popovtzer MM.** Enhanced glomerular filtration and Na^+-K^+-ATPase with furosemide administration. *Am J Physiol Renal Fluid Electrolyte Physiol* 252: F910–F915, 1987.
29. **Simon DB, Bindra RS, Mansfield TA, Nelson-Williams C, Mendonca E, Stone R, Schurman S, Nayir A, Alpay H, Bakkaloglu A, Rodriguez-Soriano J, Morales JM, Sanjad SA, Taylor CM, Pilz D, Brem A, Trachtman H, Griswold W, Richard GA, John E, Lifton RP.** Mutations in the chloride channel gene, CLCNKB, cause Bartter's syndrome type III. *Nat Genet* 17: 171–178, 1997.
30. **Simon DB, Karet FE, Hamdan JM, DiPietro A, Sanjad SA, Lifton RP.** Bartter's syndrome, hypokalaemic alkalosis with hypercalciuria, is caused by mutations in the Na-K-2Cl cotransporter NKCC2. *Nat Genet* 13: 183–188, 1996.
31. **Simon DB, Karet FE, Rodriguez-Soriano J, Hamdan JH, DiPietro A, Trachtman H, Sanjad SA, Lifton RP.** Genetic heterogeneity of Bartter's syndrome revealed by mutations in the K^+ channel, ROMK. *Nat Genet* 14: 152–156, 1996.
32. **Wang T.** Role of iNOS and eNOS in modulating proximal tubule transport and acid-base balance. *Am J Physiol Renal Physiol* 283: F658–F662, 2002.
33. **Wang T, Inglis FM, Kalb RG.** Defective fluid and HCO_3^- absorption in proximal tubule of neuronal nitric oxide synthase-knockout mice. *Am J Physiol Renal Physiol* 279: F518–F524, 2000.
34. **Watanabe S, Fukumoto S, Chang H, Takeuchi Y, Hasegawa Y, Okazaki R, Chikatsu N, Fujita T.** Association between activating mutations of calcium-sensing receptor and Bartter's syndrome. *Lancet* 360: 692–694, 2002.
35. **Weibel E.** *Stereological Methods: Practical Methods for Morphometry*. *New* York: Academic, 1979.